Supersolid phase in fully frustrated Josephson-junction arrays

Luigi Amico, Giuseppe Falci, Rosario Fazio, and Gaetano Giaquinta
Istituto di Fisica, Facoltá di Ingegneria, Universitá di Catania, viale A. Doria 6, I-95129 Catania, Italy
(Received 15 July 1996)

We study the phase diagram and the excitation spectra of an array of small Josephson junctions at $f=1/2$ and arbitrary charge frustration. We find that the supersolid region in the phase diagram is larger than the corresponding region at $f=0$ and it includes two different phases. In the chiral supersolid charges and vortices are arranged in a checkerboard pattern on a 2×2 supercell analogously to the unfrustrated case. We find a phase, which we term *nonchiral supersolid*, which has no corresponding phase at $f=0$. The excitation spectra in the supersolid regions show particlelike dispersion which is related to the existence of defectons. The defecton condensation leads to superfluidity in the presence of a charge-ordered background. [S0163-1829(97)00801-1]

I. INTRODUCTION

Josephson junctions arrays (JJA's) are ideal model systems to study a variety of phase transitions induced by thermal or quantum fluctuations.[1,2] These latter play a major role if the superconducting islands are of submicrometer size and they drive the zero-temperature superconductor-insulator (SI) phase transition. The two characteristic energy scales in the system are the Josephson energy J, which is associated with the tunneling of Cooper pairs between neighboring islands, and the charging energy U which is the energy cost to add an extra Cooper pair on a neutral island. The electrostatic energy tends to inhibit the Josephson tunneling: A finite U leads to quantum fluctuations of the phases ϕ of the superconducting order parameter $\Delta e^{i\phi_i}$, one each island. If $J\gg U$, the system is superconducting since the fluctuations of the ϕ's are small and the system is globally coherent. We will refer to the $J/U\rightarrow\infty$ limit as the *classical* case (in the classical limit JJA's are a physical realization of the two-dimensional XY model). In the opposite limit $J\ll U$, the array is a Mott insulator since strong quantum fluctuations of ϕ_i prevent the system from reaching coherence (Coulomb blockade of Cooper pairs). The SI phase transition in JJA's has been studied in great detail both experimentally[3] and theoretically.[4] The effect of disorder and the presence of an additional glass transition has been studied in Ref. 5. At the transition the system could be a metal with a universal value of the conductance.[6–8]

Frustration in a quantum JJA can be introduced either by applying a magnetic field or by means of a gate voltage with respect to the ground plane. The effect of the *magnetic frustration* has been studied extensively in the classical limit.[9] The presence of the magnetic field induces vortices in the system, and if the frustration is a rational number ($f\equiv\Phi/\Phi_0=p/q$, where Φ is the magnetic flux piercing each plaquette and $\Phi_0=h/2e$), then the ground state consists of a checkerboard configuration of vortices with a $q\times q$ elementary cell. A particularly interesting case is the fully frustrated situation ($f=1/2$) where the two degenerate ground states consist of a vortex lattice with a 2×2 elementary supercell. The current corresponding to this vortex arrangement flows either clockwise or counterclockwise in each plaquette. We refer to this ϕ configuration as a *chiral* (ground) state. The effect of quantum fluctuations in JJA's at $f=1/2$ has been investigated in Ref. 10. Although the superconducting transition temperature is reduced, the configuration of the phases ϕ_i and the supercurrent flow patterns are unchanged, and so the ground state is still chiral.

Quantum fluctuations may be modulated by means of a gate voltage to the ground V_x; this effect is known as *charge frustration*. The energy difference for two charge states in each island with n and $n+1$ extra electrons may be reduced by changing V_x. Consequently the effects of a finite charging energy are weakened and the superconducting region in the phase diagram turns out to be enlarged. In the presence of charge frustration and a finite-range Coulomb interaction, the phase diagram has a rather rich structure. Various Mott insulating phases appear. They are characterized by crystal-like configurations (with a lattice constant which depends on V_x) of the charges on the islands. In addition a new phase, characterized by the coexistence of off-diagonal (superfluid) and diagonal (charge-crystalline) long-range order, may appear. This phase is known as the *supersolid*. Since the original prediction by Andreev and Lifshitz,[11] there have been numerous works concerning the determination of the location and the size of the supersolid region as a function of the system's parameters.[12–15] Most of these theoretical investigations employ the mean field approximation. Recently quantum Monte Carlo calculations were performed in Ref. 16 for the JJA model and in Ref. 17 for the Bose-Hubbard model. These simulations confirmed the existence of the supersolid region although its size is substantially reduced compared to the mean field estimates. Investigations in one-dimensional systems[18] by means of Monte Carlo simulations do not show any trace of the supersolid.

All these investigations concerning the effect of frustration in quantum arrays considered either charge *or* magnetic frustration. The combined effect of *both* types of frustration may lead to interesting effects. The most striking prediction is that for certain ratios of the magnetic to charge frustration the JJA is in a quantum Hall phase.[19] The proposal is rather suggestive, although experiments are not yet available to support it and there is no detailed study of the phase diagram

which would allow one to locate the region where the quantum Hall phase should be observed.

Motivated by these recent developements, we study in this work the phase diagram and the low-lying excitations of a JJA in the presence of both charge and magnetic frustration. In particular we consider the case of fully frustrated JJA's for which the ground state is known in the classical limit. Two different supersolid phases are identified which we indicate as *chiral* supersolid (SS) and *nonchiral* supersolid (NCSS). This NCSS is a new phase and has no corresponding stable phase at $f=0$. The *whole* supersolid region is enlarged as compared to the case of zero magnetic field.

The paper is organized as follows. In the next section we introduce the quantum phase model (QPM) commonly used to study JJA's and reduce it in the standard way to the XXZ Heisenberg model. The phase diagram of the latter model is studied at the mean field level in Sec. III using the $1/S$ expansion. We would like to point out that the presence of both magnetic and charge frustrations makes the calculation nontrivial already at this level and that it is impossible to use other standard tools such as Monte Carlo simulations or the self-consistent harmonic approximation. In the case of Monte Carlo calculations there is the sign problem (due to the combined effect of both types of frustration) while in the harmonic approximation the discreteness of charges which is essential to describe supersolids is lost. In Sec. IV we study the spectrum of the low-lying excitations in all the regions of the phase diagram. Finally, Sec. V is devoted to the conclusions.

II. MODEL

In quantum JJA's the only relevant dynamical variables are the phases ϕ_i defined on each island (at low temperatures the fluctuations of the modulus Δ are unimportant). Since in nanofabricated samples there are no Ohmic currents between the islands and also quasiparticle tunneling is negligible, all the physics is captured by the QPM ($\hbar=1$)

$$H_{\mathrm{QP}}=\frac{1}{2}\sum_{i,j}(n_i-n_x)U_{ij}(n_j-n_x)-J\sum_{\langle i,j\rangle}\cos(\phi_i-\phi_j-A_{ij}), \tag{1}$$

where n_i (the charge on the ith island) is canonically conjugated to ϕ_i, $[\phi_i,n_j]=2ei\delta_{ij}$. The Coulomb interaction is described by the matrix $U_{ij}=4e^2C_{ij}^{-1}$, where C_{ij} is the capacitance matrix. The external voltage V_x enters via the induced charge en_x and fixes the average charge on each island. A perpendicular magnetic field with vector potential $\mathbf{A}$ enters the QPM in the standard way through $A_{ij}=(2e/c)\int_i^j\mathbf{A}\cdot d\mathbf{l}$. The relevant parameter which describes the magnetic frustration is $f=(1/2\pi)\Sigma A_{ij}$, where the summation runs on an elementary plaquette.

In the case of a very large *on-site* Coulomb interaction and very low temperatures only a few charge states are important. If the gate voltage is tuned close to a degeneracy, the relevant physics is captured by considering only two charge states per island and the QPM is equivalent to a spin-1/2 Heisenberg model[12]

$$H_S=-h\sum_i S_i^z+\tfrac{1}{2}\sum_{i,j}S_i^zU_{ij}S_j^z$$

$$-J\sum_{\langle i,j\rangle}(e^{iA_{ij}}S_i^+S_j^-+e^{-iA_{ij}}S_j^+S_i^-), \tag{2}$$

where the operators S_i^z, S_i^+, and S_j^- are the usual su(2) operators, S_i^z being related to the charge on each island ($n_i=S_i^z+1/2$), and the raising and lowering $S_i^{\pm}$ operators corresponding to the operators $e^{\pm i\phi_j}$ of the QPM. The fictitious external field h is related to the external charge by

$$h=(n_x-1/2)\sum_j U_{i,j}.$$

The various magnetic orderings in the XXZ Hamiltonian correspond to the different phases in the QPM.

(i) Long range order in $\langle S^x\rangle$ and $\langle S^y\rangle$ ($\sqrt{\langle S^x\rangle^2+\langle S^y\rangle^2}\neq 0$) indicates superfluidity in the QPM.

(ii) Long range order in $\langle S^z\rangle$ ($|\langle S^z\rangle|\neq 0$) describes order in the charge configuration.

In the rest of the paper we consider the Coulomb interaction only between nearest-neighbor (NN) (U_1) and next-nearest-neighbor (NNN) (U_2) sites.

III. PHASE DIAGRAM

In this section we obtain the phase diagram for $f=1/2$ in the presence of arbitrary charge frustration. Previous work already established the phase diagram of the spin Hamiltonian for zero magnetic frustration ($f=0$).[12–14,17]

We consider a square lattice and use the gauge $\mathbf{A}=Hy\hat{\mathbf{x}}$. This gives $A_{ij}=\pi(y_i/a)\mathrm{sgn}(x_j-x_i)$ where the coordinates of the neighboring sites i and j appear and a is the lattice spacing. This is illustrated in Fig. 1 where the dashed lines indicate the antiferromagnetic bond ($A_{ij}=\pi$) and the solid lines the ferromagnetic bonds ($A_{ij}=0$).

In the classical limit there are two degenerate 2×2 periodic ground states: In the QPM language the corresponding ϕ_i configurations describe a checkerboard arrangement of vortices and antivortices. In XXZ language the spin components are related to ϕ by $\arctan(\langle S_i^y\rangle/\langle S_i^x\rangle)=\phi_i$ and $\sqrt{\langle S_i^x\rangle^2+\langle S_i^y\rangle^2}=1$. In the classical limit charges are completely delocalized which implies $\langle S_i^z\rangle=0$.

The chiral configuration of the classical ground states suggests the introduction of four sublattices indicated by the index $l=\alpha,\beta,\gamma,\delta$ (Fig. 1). Each site is parametrized by l and an additional index p which runs, within each sublattice, through the whole array.

We study the XXZ model using the $1/S$ expansion (S is the modulus of the spin vector). First the quantization axis in each sublattice is rotated to align the spins along the direction of the relative magnetization. We obtain the rotated Hamiltonian $\mathbf{R}H_S\mathbf{R}^{-1}$, where

$$\mathbf{R}\doteq\prod_p\prod_{l=\alpha,\beta,\gamma\delta}R^z{}_{pl}R^x{}_{pl}, \tag{3}$$

with $R^z{}_{pl}\doteq e^{i\phi_lS^z_{pl}}$ and $R^x{}_{pl}\doteq e^{i\theta_lS^x_{pl}}$. Then we perform the $1/S$ expansion and determine the actual values of the eight angles ϕ_l and θ_l by minimizing the $S\to\infty$ limit of the rotated

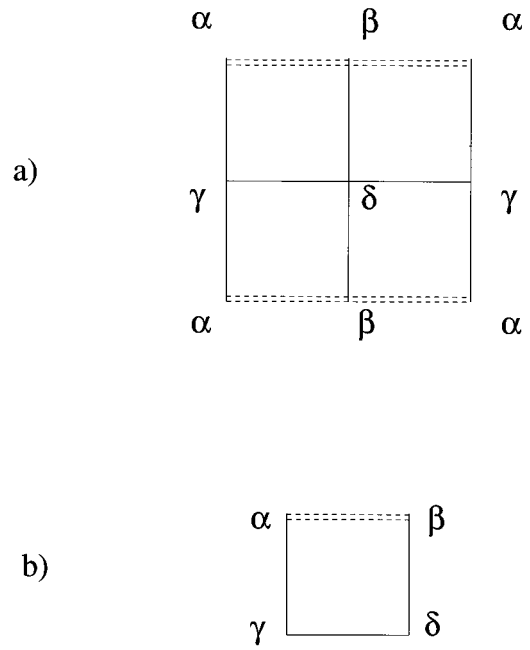

FIG. 1. Because of the nontrivial periodicity due to the magnetic frustration, a 2×2 cell should be considered. The labels for the sites as used in the paper are here reported (a). Using periodicity boundary conditions, as shown in (a), one can reduce the problem defined on the plaquette drawn in (b).

Hamiltonian. The above procedure allows us to characterize ground states whose properties are uniform within each sublattice (the angles θ and ϕ do not depend on the subscript p).

At the mean field level the order parameters are $\sin\theta_l$ for global phase coherence (off-diagonal order) and $\cos\theta_l$ for charge ordering (diagonal order). The ϕ_l configuration determines the supercurrent pattern. The $1/S$ expansion of the rotated Hamiltonian can be carried on systematically by using the Holstein-Primakoff transformation $S^+_{pl}=\sqrt{2S}a^\dagger_{pl}\sqrt{1-n_{pl}/S}$, $S^-_{pl}=(S^+_{pl})^\dagger$, $S^z_{pl}=n_{pl}-S$, where a_{pl} and $a^\dagger_{pl}$ are boson operators, and $n_{pl}=a^\dagger_{pl}a_{pl}$. These operators describe excitations around the $S\to\infty$ ground state. The rotated Hamiltonian reads

$$\mathbf{R}H_S\mathbf{R}^{-1}=H_\infty+H_{SW}+\mathcal{O}(\sqrt{S}), \tag{4}$$

where H_∞ is of order S^2, and H_{SW} describes low-energy fluctuations around the $S\to\infty$ ground state and turns out to be of order S. The $S\to\infty$ ground-state properties are obtained by minimizing H_∞:

$$H_\infty=\frac{N}{4}\sum_l\Bigg[-\frac{h}{2}\cos\theta_l+\frac{U_1}{8}\cos\theta_l\sum_{m=\mathrm{NN}(l)}\cos\theta_m+\frac{U_2}{4}\cos\theta_l\sum_{m=\mathrm{NNN}(l)}\cos\theta_m-\frac{J}{4}\sin\theta_l\sum_{m=\mathrm{NN}(l)}e^{A_{lm}}\sin\theta_m\cos(\phi_l-\phi_m)\Bigg]. \tag{5}$$

The minimization of the H_∞ leads to eight equations in the variables ϕ_l and θ_l defined on the plaquette of Fig. 1(b). Four of these equations can be solved analytically with the result

$$\tan(\phi_\gamma-\phi_\beta)=\frac{\sqrt{16a^2b^2-(b^2-1)(a^2-1)}}{(b^2-1)(a^2+1)},$$

$$\tan(\phi_\delta-\phi_\alpha)=-\frac{\sqrt{16a^2b^2-(b^2-1)(a^2-1)}}{(a^2-1)(b^2+1)},$$

$$\tan(\phi_\beta-\phi_\alpha)=-\frac{\sqrt{16a^2b^2-(b^2-1)(a^2-1)}}{(a^2-1)(b^2+1)-2b^2(a^2+1)}, \tag{6}$$

where

$$a=\frac{\sin\theta_\alpha}{\sin\theta_\delta},\quad b=\frac{\sin\theta_\beta}{\sin\theta_\gamma}$$

(the solutions are valid if a and b are both finite). We now look for solutions with $a=b=1$ which correspond to phases with checkerboard symmetry. The resulting configuration of the ϕ_l is the same as in the classical limit, and the supercurrent has the same chiral pattern. This has been noticed in the case of zero external charge in Ref. 10. We show that, for nonzero charge frustration, the above conclusion is also valid for the superfluid phase and for the chiral SS.

The remaining equations for θ_l reduce to the ones of the $f=0$ case with the substitution $J\to J/\sqrt{2}$. The solutions then read

$$\cos\theta=\frac{h}{2(U_1+U_2+\sqrt{2}J)} \tag{7}$$

for the superfluid (SF) and

$$\cos\theta_{\alpha,\beta}=\tfrac{1}{2}(v\pm\sqrt{v^2-4w})$$

for the chiral SS. We defined

$$w\doteq(h-h_s)/(2U_2\kappa),\quad h_s\doteq2\sqrt{(U_1-U_2)^2-2J^2}$$

$$\kappa\doteq\sqrt{1-[\sqrt{2}J/(U_1-U_2)]^2}(1+w),$$

and

$$v=\kappa(1+w).$$

By comparing the energies relative to the above solutions we obtain the boundaries between the phases with checkerboard symmetry.

Paramagnetic-canted state:

$$h=\pm2(U_1+U_2+\sqrt{2}J). \tag{8}$$

Canted state, $\frac{1}{4}$ or $\frac{3}{4}$ lobe:

$$h=\pm[U_1+U_2+\sqrt{2}J+\sqrt{(U_1+U_2+\sqrt{2}J)(U_1+U_2-3\sqrt{2}J)}]. \tag{9}$$

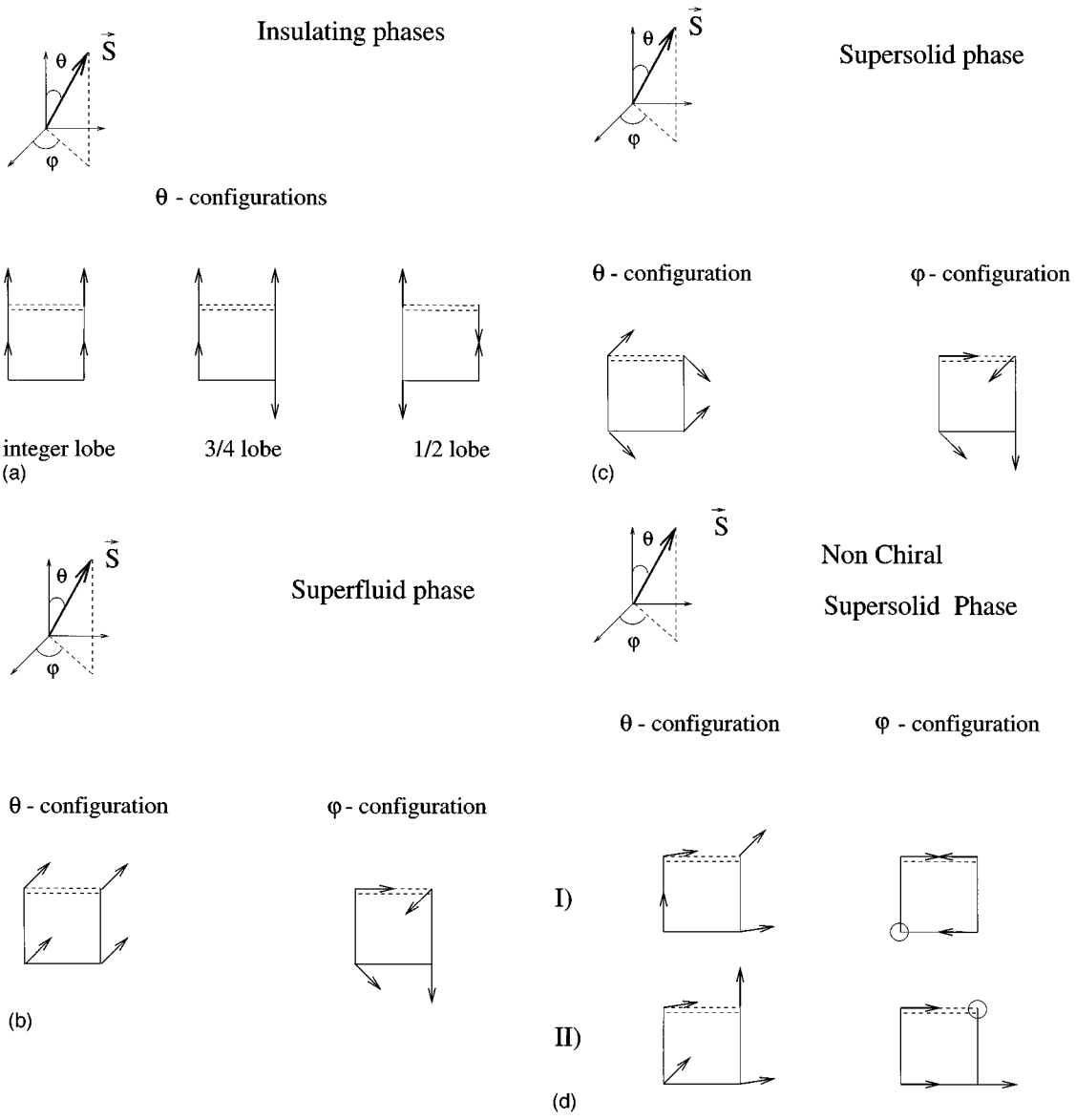

FIG. 2. The three-components spin vectors we used are characterized by the usual Euler angles θ and ϕ. (a) In the insulating phases the order parameter vanishes and only the θ configuration is important. (b) The mean field order parameter's phase configuration is unaffected by magnetic frustration. (c) The θ and ϕ configurations in the SS. As in the superfluid state, the magnetic frustration preserves the chiral order of the ground state. (d) The two degenerate ground states of the NCSS. The circle indicates the lattice site where the phase of the superfluid order parameter is not defined (the two degenerate configurations both refer to the case $a=1$).

Canted–chiral-supersolid state:

$$h=2(U_1+U_2+\sqrt{2}J)\sqrt{\frac{(U_1-U_2-\sqrt{2}J)}{(U_1-U_2+\sqrt{2}J)}}. \qquad (10)$$

Chiral-supersolid–Néel state:

$$h=2\sqrt{(U_1-U_2)^2-2J^2}. \qquad (11)$$

Chiral supersolid, $\frac{1}{4}$ or $\frac{3}{4}$ lobes:

$$h=\pm[2U_2+h_s-\sqrt{(2U_2+h_s)^2-h_s{}^2-8U_2(U_1-U_2)}]. \qquad (12)$$

The spin configurations corresponding to the insulating, superfluid and supersolid regions are shown in Fig. 2. In the Mott lobes there is no projection of the spin on the xy plane and the three spin configurations in Fig. 2(a) correspond to filling 1, 1/2, and 3/4. In Fig. 2(b) and Fig. 2(c) the superfluid and supersolid configurations are represented. The fact that the ϕ configuration is not affected by quantum fluctuations has already been noticed in Ref. 10 for zero external charge. We extend this result to the SF and SS phases. However, we discuss below a new phase, the *nonchiral supersolid*, which shows a different supercurrent pattern.

The NCSS ground state is found when we look for solutions with no checkerboard symmetry which minimize Eq. (5). (A noncheckerboard phase was also found at $f=0$ by Bruder *et al.*[14] and was named a SS2 supersolid.) We choose $a=1$ and $b\neq 1$ (or equivalently $a\neq 1$ and $b=1$). In this case the ground state has the following phase configurations:

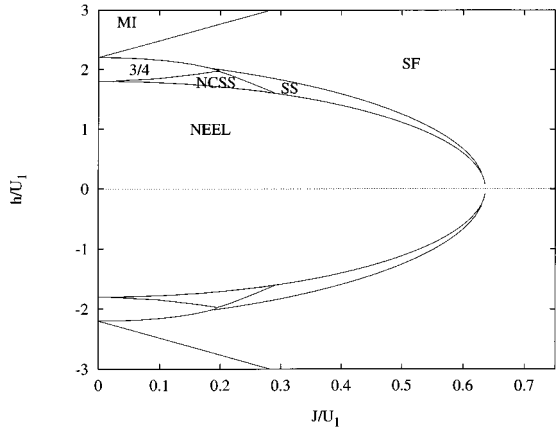

FIG. 3. The phase diagram for the fully frustrated JJA. The NNN Coulomb interaction is $U_2=0.1U_1$.

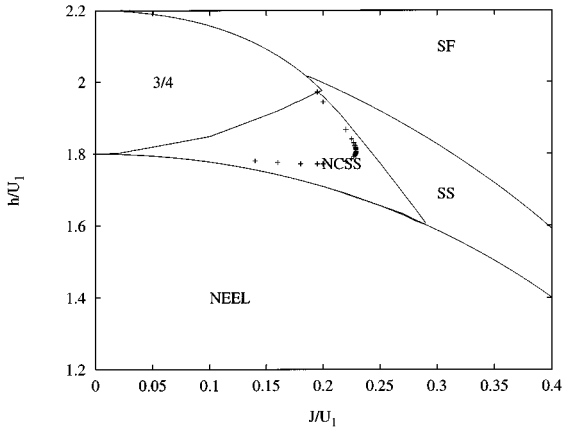

FIG. 4. The region of the phase diagram containing the NCSS is shown in detail. In addition we report (with crosses) the phase boundary that should have the chiral SS2 by rescaling J as discussed in the text.

$$\phi_\alpha=0,$$

$$\phi_\beta=\phi_\gamma+\pi/2,$$

$$\phi_\delta=2\phi_\gamma,$$

and

$$\phi_\gamma=\arctan b.$$

Substituting these values of the phases in H_∞ and by numerical minimization of the corresponding expression of H_∞, we find two degenerate NCSS configurations

$$\phi_\alpha=0,\phi_\beta=\phi_\delta=\pi$$

($\sin\theta_\gamma=0$) and

$$\phi_\alpha=\phi_\gamma=\phi_\delta=0$$

($\sin\theta_\beta=0$). In the previous expressions, ϕ_γ [for the configuration of Fig. 2(dI)] and ϕ_β [for the configuration of Fig. 2(dII)] are meaningless since the superfluid order parameter is zero in this site.

The resulting pattern of supercurrent is different from the classical chiral one. We point out that in this case the equations for the angles θ_l cannot be obtained from the $f=0$ equations by simply rescaling $J\to J/\sqrt{2}$.

The solutions are characterized by the $\sin\theta$ order parameter vanishing on one of the four sublattices. On this particular sublattice $\cos\theta=1$, and so the charge is well defined. Thus the NCSS ground state describes a supersolid, since charge-crystalline and superfluid order coexist, but the chiral supercurrent pattern is lost.

All the phase boundaries obtained in this section are summarized in the phase diagram shown in Fig. 3. The *whole* supersolid region (SS and NCSS phases) is enlarged compared to the $f=0$ case (SS1 and SS2 phases). At $f=0$ the tip of the lobe (which coincides with the extension of the supersolid phase in the hard core limit) will correspond to $J/U_1=0.45$. A blowup of the NCSS region is shown in Fig. 4 and compared with the rescaled $f=0$ phase diagram. This figure emphasizes that the *whole* supersolid region cannot be obtained by rescaling the $f=0$ phase diagram (the rescaled SS2-SS1 phase boundary is shown by crosses).

IV. EXCITATION SPECTRA

The excitation spectra can be obtained calculating the eigenmodes of H_{SW}. As pointed out in the previous section all the terms up to $\mathcal{O}(S)$ are retained in the $1/S$ expansion; this, in turn, corresponds to retaining products at most bilinear of the creation and annihilation operators $a^\dagger$ and a. By considering l as a color index, H_{SW} describes a system of four kinds of interacting bosons defined on a lattice whose sites are labeled by the index p. Then we Fourier transform with respect to p and H_{SW} reduces to a sum of single-mode Hamiltonians

$$H_{SW}=\sum_k H_k,$$

$$\begin{aligned}H_k=&(\varepsilon_k^{(\alpha,\beta)}+\varepsilon_k^{(\alpha,\gamma)}+\varepsilon_k^{(\alpha,\delta)})n_{k,\alpha}+(\varepsilon_k^{(\alpha,\beta)}+\varepsilon_k^{(\beta,\delta)}+\varepsilon_k^{(\beta,\gamma)})n_{k,\beta}+(\varepsilon_k^{(\alpha,\gamma)}+\varepsilon_k^{(\gamma,\delta)}+\varepsilon_k^{(\beta,\gamma)})n_{k,\gamma}+(\varepsilon_k^{(\alpha,\delta)}+\varepsilon_k^{(\beta,\delta)}+\varepsilon_k^{(\gamma,\delta)})n_{k,\delta}\\
&+(v_k^{(\alpha,\gamma)}a_{k,\alpha}^\dagger a_{k,\gamma}+v_k^{(\alpha,\gamma)*}a_{k,\gamma}^\dagger a_{k,\alpha})+(v_k^{(\alpha,\beta)}a_{k,\alpha}^\dagger a_{k,\beta}+v_k^{(\alpha,\beta)*}a_{k,\beta}^\dagger a_{k,\alpha})+(v_k^{(\beta,\delta)}a_{k,\beta}^\dagger a_{k,\delta}+v_k^{(\beta,\delta)*}a_{k,\delta}^\dagger a_{k,\beta})\\
&+(v_k{}^{(\gamma,\delta)}a_{k,\gamma}^\dagger a_{k,\delta}+v_k^{(\gamma,\delta)*}a_{k,\delta}^\dagger a_{k,\gamma})+(v_k^{(\alpha,\delta)}a_{k,\alpha}^\dagger a_{k,\delta}+v_k^{(\alpha,\delta)*}a_{k,\alpha}^\dagger a_{k,\delta})+(v_k^{(\beta,\gamma)}a_{k,\beta}^\dagger a_{k,\gamma}+v_k^{(\beta,\gamma)*}a_{k,\gamma}^\dagger a_{k,\beta})\\
&+(q_k^{(\alpha,\gamma)}a_{k,\alpha}^\dagger a_{k,\gamma}^\dagger+q_k^{(\alpha,\gamma)*}a_{k,\gamma}a_{k,\alpha})+(q_k^{(\alpha,\beta)}a_{k,\alpha}^\dagger a_{k,\beta}^\dagger+q_k^{(\alpha,\beta)*}a_{k,\beta}a_{k,\alpha})+(q_k^{(\beta,\delta)}a_{k,\beta}^\dagger a_{k,\delta}^\dagger+q_k^{(\beta,\delta)*}a_{k,\beta}a_{k,\delta})\\
&+(q_k^{(\gamma,\delta)}a_{k,\gamma}^\dagger a_{k,\delta}^\dagger+q_k^{(\gamma,\delta)*}a_{k,\gamma}a_{k,\delta})+(q_k^{(\alpha,\delta)}a_{k,\alpha}^\dagger a_{k,\delta}^\dagger+q_k^{(\alpha,\delta)*}a_{k,\alpha}a_{k,\delta})+(q_k^{(\beta,\gamma)}a_{k,\beta}^\dagger a_{k,\gamma}^\dagger+q_k^{(\beta,\gamma)*}a_{k,\gamma}a_{k,\beta}).\end{aligned}\tag{13}$$

The coefficients in the Hamiltonian (13) (reported in Appendix A) depend on the angles θ_l and ϕ_l introduced in Sec. III. The k sum is restricted to half of the Brillouin zone because of the doubling of the lattice constant due to the magnetic frustration. All the linear terms in the operators $a^\dagger_{k,i}$ and $a_{k,i}$ vanish for the $\{\theta_l,\phi_l\}$ configurations in the ground state.

The Hamiltonian H_{SW} is diagonalized using an algebraic technique[20,21,28,29] briefly described below: We introduce the operators

$$
\begin{aligned}
X_{ll'} &\doteq a_{k,l}a_{-k,l'}+a_{k,l'}a_{-k,l},\\
X^{ll'} &\doteq a^\dagger_{k,l'}a^\dagger_{-k,l}+a^\dagger_{k,l}a^\dagger_{-k,l'}=(X_{ll'})^\dagger,\\
X_l{}^{l'} &\doteq a^\dagger_{k,l'}a_{k,l}+a^\dagger_{-k,l'}a_{-k,l},\\
X_{l'}{}^{l} &\doteq a^\dagger_{k,l}a_{k,l'}+a^\dagger_{-k,l}a_{-k,l'}=(X_l{}^{l'})^\dagger,\\
X_l{}^{l} &\doteq n_{k,l}+n_{-k,l}+1,
\end{aligned}
\tag{14}
$$

which obey the commutation rules

$$
\begin{aligned}
&[X_{ll'},X_{mm'}]=[X^{ll'},X^{mm'}]=0,\\
&[X_{ll'},X^{mm'}]=X_l{}^m\delta_{l'}{}^{m'}+X_l{}^{m'}\delta_{l'}{}^m+X_{l'}{}^m\delta_l{}^{m'}+X_{l'}{}^{m'}\delta_l{}^m,\\
&[X_{ll'},X_m{}^{m'}]=X_{lm}\delta_{l'}{}^{m'}+X_{l'm}\delta_l{}^{m'},\\
&[X^{ll'},X_m{}^{m'}]=-X^{lm'}\delta_m{}^{l'}-X^{l'm'}\delta_m{}^l,\\
&[X_l{}^{l'},X_m{}^{m'}]=X_m{}^{l'}\delta_l{}^{m'}-X^{lm'}\delta_m{}^{l'},
\end{aligned}
\tag{15}
$$

where we have omitted the k index in the X's and $\{l,l',m,m'\}$ are the color indices. The 36 operators $\{X_{ll'},X^{ll'},X_l{}^{l'},X_{l'}{}^l,X_l{}^l\}$ form a base for the noncompact symplectic Lie algebra $\mathrm{sp}(8)_k$.[22] The diagonal operators in the Foch base $X_l{}^l$ generate the Cartan subalgebra of $\mathrm{sp}(8)_k$ whose dimension is 4 (equal to the rank of the algebra). The other 32 off-diagonal operators are the non-Cartan generators of the algebra. By using the definitions of Eq. (14), one can see that H_k belongs to $\mathrm{sp}(8)_k$ since it can be written as a linear combination of a subset of its generators:

$$
H_k=\sum_l D^{(k)}_{ll}X_l{}^l+\sum_{l\neq l'}D_{ll'}{}^{(k)}X_l{}^{l'}+\sum_{l\neq l'}R_{ll'}{}^{(k)}X_{ll'},
\tag{16}
$$

where $R_{ll'}{}^{(k)}=R_{l'l}{}^{(k)*}$ and $D_{ll'}{}^{(k)}=D_{l'l}{}^{(k)*}$. The coefficients in expression (16) are listed in Appendix B. Equation (16) suggests that H_{SW} possesses $\mathcal{A}=\oplus_k\mathrm{sp}(8)_k$ as dynamical algebra; therefore we can diagonalize the Hamiltonian using the fundamental, faithful (i.e., preserving the commutation rules) irreducible representation (IRR) of $\mathcal{A}$. It is worthwhile to notice that because of the noncompactness of $\mathrm{sp}(8)$, every finite-dimensional IRR of such an algebra is not Hermitian.[23] Despite this fact we can use the IRR of $\mathcal{A}$ in order to obtain the correct eigenvalues of H_{SW} (see Appendix A). Such eigenvalues still depend on θ_l and ϕ_l: The actual spectra in the various phases are worked out by specifying the corresponding $S\to\infty$ ground-state $\{\theta_l\phi_l\}$ configuration for each phase. The main results of this procedure are described below for the various regions of the phase diagram.

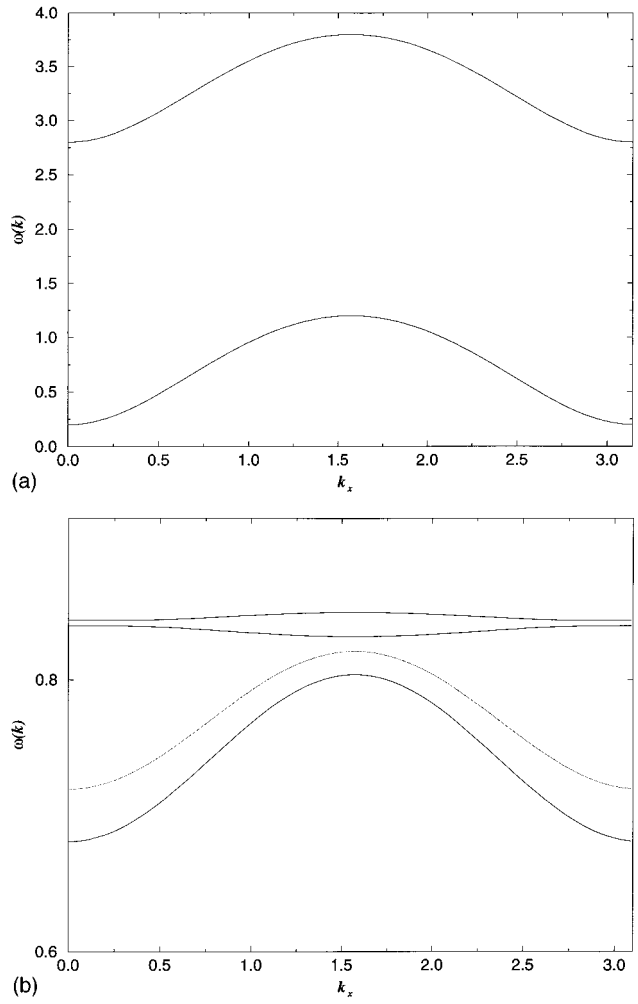

FIG. 5. (a) The excitation spectrum of the Néel insulator. At $J=U_1/4$, $U_2=3U_1/8$ and $h=2U_1/3$. The behavior at small k reveals the particlelike nature of the excitations. In (b) we show the four branches of the ''3/4'' insulating phase ($U_2=0.1U_1$, $h=2U_1$, and $J=0.1U_1$). The two lower curves have been rescaled by a factor of 10.

Insulating phases. Since the superfluid order parameter is zero, there is no effect due to magnetic frustration. The Néel and insulating 1/4 (and 3/4) phases are charge-modulated solids. The lowest-lying excitations are gaped and particlelike. They correspond to particle-hole excitations. In Fig. 5(a) and Fig. 5(b) we show the spectrum for the 1/2 and 3/4 lobes. The Néel solid is charge modulated along both x and y directions and the excitation branches are shown in Fig. 5(a). The four branches in the 3/4 lobe come from the more complicated structure of the elementary cell. In this state there is a transverse-phononlike excitation, characteristic of the diagonal long-range order along rows and/or columns (where the charge is uniform). In addition we find the particlelike spectrum (with positive curvature at small k) which reflects charge modulation. This is shown in Fig. 5(b) where the branch with negative curvature, represents the phononlike excitation.

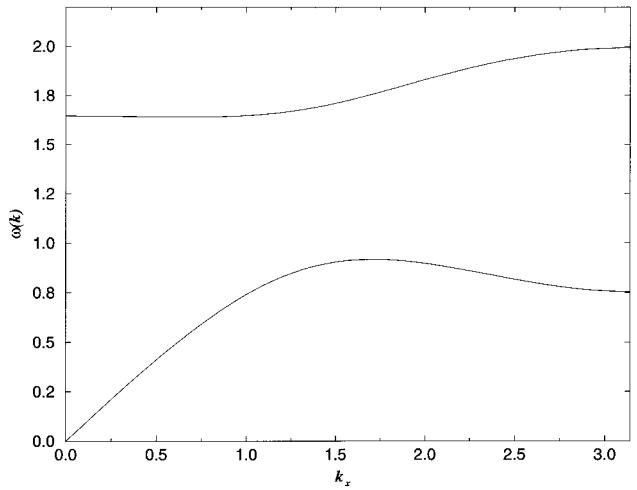

FIG. 6. The acoustic- and transverse-phononlike branches in the superfluid are shown for $J=U_1$, $U_2=0.1U_1$, $h=2.2U_1$, and $k_y=0$.

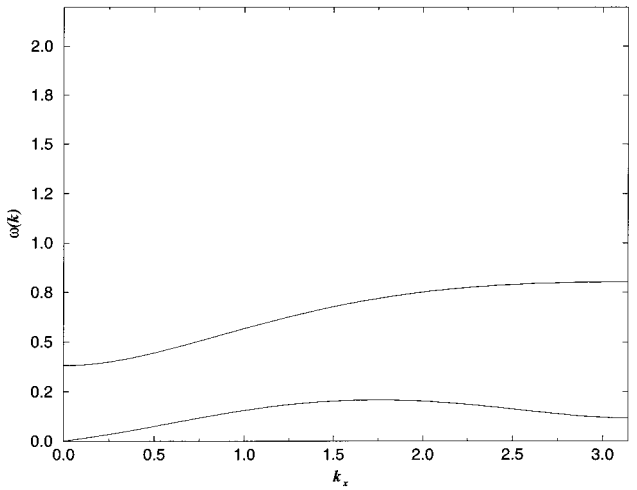

FIG. 7. In this figure we show the dispersion relations in the SS ($J=0.35U_1$, $U_2=0.1U_1$, $h=1.7U_1$, and $k_y=0$). The sound velocity of the acoustic branch is reduced compared to the superfluid case. The gapped branch has a positive curvature at small k characteristic of the particlelike nature of the excitations.

The Mott phases are not modulated in any direction, and then the low-lying excitations are phononlike.

SF phase: Because of the doubling of the elementary cell of the lattice due to the magnetic frustration, an optical branch is present in addition to a gapless mode which linearly depends on k at small k; see Fig. 6. This was already discussed in the classical case by Ariosa *et al.*[9] Long-range diagonal order existing along any lattice direction induces transverse-phononlike excitations.

Supersolid SS *phase*: In the SS phase both diagonal and off-diagonal order modulations are present. In this state the in-phase density fluctuations are coupled to the off-diagonal fluctuations and decrease the sound velocity because they reduce the superfluid density. The supersolid is characterized also by a modulation of the charge. Such modulation of the number of particles can be described in terms of defects of the lattice and the oscillations of the particles lead to fluctuations in the diagonal order on each site.[24] The localized quasiparticles associated with the collective oscillations of the defects were termed *defectons*.[11] The branch with a gap reveals the particlelike excitations consistently with this physical picture. In Fig. 7 the acoustic branch is reminiscent of the superfluid order while the gapped branch with positive curvature corresponds to the excitation spectrum of the defectons.

NCSS phase: As in the previous case, the off-diagonal order is coupled with the density waves, but in this state there are four branches. The gapless one reflects the superfluid nature of this state. Since the mean field superfluid order parameter vanishes in a lattice site of the 2×2 plaquette, the sound velocity is strongly decreased. Two of the three gapped curves take into account the defects of the lattice; the other one means that in the system there are transverse phase-phonon excitations too. This is summarized in Fig. 8.

An important issue which can be addressed by studying the excitation spectrum is the determination of the dynamical critical exponent at the various phase boundaries. It turns out that the fully frustrated system has the same dynamical critical exponents at the various phase boundaries as the unfrustrated one. At the SS-Néel solid transition (see Fig. 9) the gap of the lower branch of the solid vanishes as k^2, giving a critical exponent $z=2$.[17,27] At the SF-SS transition (see Fig. 10) the critical mode is $k=(\pi,\pi)$ and the roton minimum is at this wave vector. At the phase boundary the roton gap disappears linearly in k, giving $z=1$.

V. CONCLUSIONS

In this paper we discussed the properties of a fully frustrated quantum Josephson-junction array in the presence of arbitrary charge frustration. We determined the mean field phase diagram at $T=0$ as well as the low-lying excitation spectrum using a $1/S$ expansion for the equivalent XXZ model.

At $f=1/2$ two kinds of supersolid phases, in addition to the ordinary superfluid and insulating phases, are present. Besides the chiral SS which has an analogue in the absence

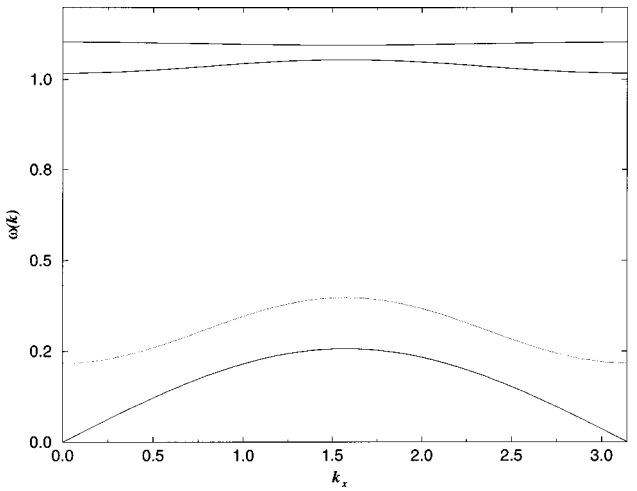

FIG. 8. The excitation spectrum of the NCSS phase ($J=0.2U_1$, $U_2=0.1U_1$, $h=1.848U_1$, and $k_y=0$). The two lower curves have been rescaled by a factor of 5.

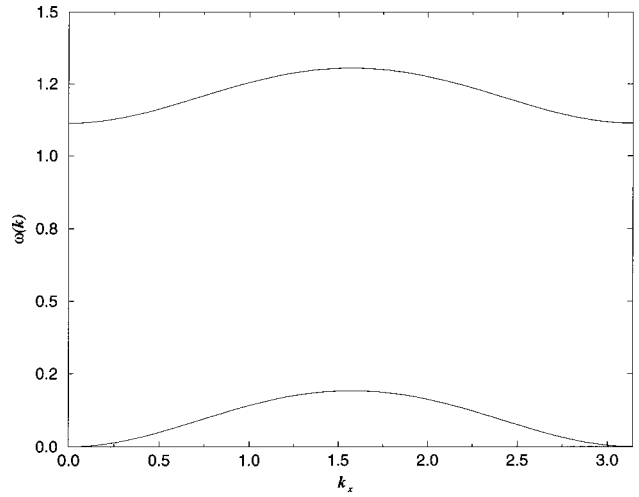

FIG. 9. At the phase boundary between the Néel insulator and SS the excitation spectrum vanishes as k^2. The transition is signaled by softening of the acoustic branch proper of the supersolid ($J=0.1U_1$, $U_2=0.1U_1$, and $k_y=0$).

of magnetic frustration we find the new NCSS phase which has a nonchiral ground state. In the case of the superfluid and the SS the main effect of quantum fluctuation and charge frustration is to lower in magnitude the superfluid order parameter. The supercurrent pattern induced by the external magnetic field is, however, unaffected. In our mean field analysis this is reflected in a rescaling of J. In other words the magnetic frustration fixes the current distribution while the charge frustration is responsible for the reduction of the magnitude of the superfluid order parameter. In the NCSS diagonal and off-diagonal long-range order coexist in a nontrivial way and the combined effect of charge and magnetic frustration cannot be disentangled as in the other phases. The NCSS ground state has no checkerboard symmetry since the superfluid order parameter vanishes in one of the four sites of each plaquette and two flux quanta may be accommodated in four neighboring plaquettes. The NCSS phase exists only in the fully frustrated case and has no analogue at $f=0$. The

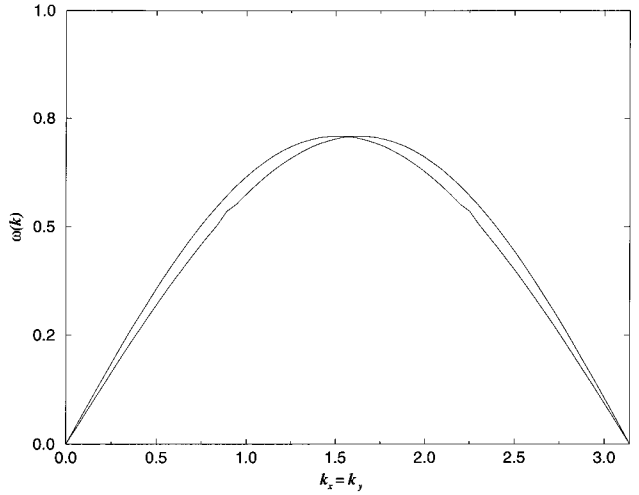

FIG. 10. At the superfluid-SS phase transition the roton mode vanishes as k ($J=0.5U_1$, $U_2=0.1U_1$, and $k_x=k_y$).

whole SS plus NCSS region in the phase diagram is enlarged compared to the unfrustrated case: The supersolid state better adjusts to the periodicity (on a 2×2 plaquettes elementary cell) induced by magnetic frustration than the SF phase and it is more favored than in the $f=0$ case. This may be important for experiments because the combination of charge and magnetic frustration may help in detecting the supersolid phase.

We also determined the low-lying excitation spectrum of the system. Due to the combined presence of magnetic and charge frustration, the excitation spectra become more structured. They can be revealed, for instance, by studying the anomalies in the *I-V* characteristics in the Andreev current when the array is coupled to a normal metal electrode.[25]

We are currently investigating different rational values of the magnetic frustration in order to study the possibility of a quantum Hall phase as predicted in Ref. 19.

Note added in proof. After the submission of this paper, we became aware of papers by C. Murthy, D. Arovas, and A. Auerbach [Phys. Rev. B (to be published)] and by E. Frey and L. Balents [this issue, Phys. Rev. B **55**, 1050 (1997)] where similar problems are investigated.

ACKNOWLEDGMENTS

We would like to thank C. Bruder, A. van Otterlo, K.H. Wagenblast, M. Rasetti, G. Schön, and G.T. Zimanyi for useful discussions. The financial support of the European Community (HCM-network CHRX-CT93-0136) and of INFM (Italy) is gratefully acknowledged. Two of us (R.F and G.F.) acknowledge the warm hospitality of the Institut für Theoretische Festkörperphysik (Karlsruhe) where part of the work was performed.

APPENDIX A

In this appendix we list the coefficients of the Hamiltonian in Eq. (13):

$$\varepsilon_k^{(l,m)} \doteq 2te^{iA_{lm}}\sin\theta_l\sin\theta_m\cos z_{l,m} - U_1\cos\theta_l\cos\theta_m\,,$$

$$\varepsilon_k^{(l,n)} \doteq -2U_2\cos\theta_l\cos\theta_m\,. \tag{A1}$$

The coefficients of the off-diagonal operators are

$$v_k^{(l,m)} \doteq \cos(\mathbf{k}\cdot\mathbf{a}_{l,m})\left\{ te^{iA_{lm}}[(\cos\theta_l\cos\theta_m+1)\cos z_{l,m} - i(\cos\theta_l+\cos\theta_m)\sin z_{l,m}] + \frac{U_1}{2}\sin\theta_l\sin\theta_m \right\},$$

$$v_k^{(l,n)} \doteq U_2\cos k_y\cos k_x\sin\theta_l\sin\theta_m\,,$$

$$q_k^{(l,m)} \doteq \cos(\mathbf{k}\cdot\mathbf{a}_{l,m})\left\{ te^{iA_{lm}}[(\cos\theta_l\cos\theta_m-1)\cos z_{l,m} + i(\cos\theta_l+\cos\theta_m)\sin z_{l,m}] + \frac{U_1}{2}\sin\theta_l\sin\theta_m \right\},$$

$$q_k^{(l,m)} \doteq -U_2\cos k_y\cos k_x\sin\theta_l\sin\theta_m\,, \tag{A2}$$

where m and n are, respectively, NN and NNN to the site l. In the previous expression $\mathbf{a}_{l,m}$ is the unit vector joining the sites l and m and $z_{l,m} \doteq (\phi_l - \phi_m)$. The coefficients (A2) are **C** numbers; they become real only if $f=0$.

APPENDIX B

The IRR faithful representation of sp(8) we used consists in mapping the Hamiltonian H_{SW} in the matrix $\mathcal{M}(H_{SW})$. Since that sp(8) is a noncompact algebra, $\mathcal{M}$ turns out to be not Hermitian and it has the structure (we use the same notation as in Ref. 26)

$$\begin{pmatrix} \mathcal{D} & \mathcal{R} \\ -\mathcal{R} & -\widetilde{\mathcal{D}} \end{pmatrix}, \tag{B1}$$

where the tilde indicates the reflection in the minor diagonal ($\widetilde{\mathcal{R}}=\mathcal{R}$) and $\mathcal{D}$ is Hermitian. The matrix elements of $\mathcal{D}$ are

$$\begin{aligned} D_{11}{}^{(k)} &\doteq \tfrac{1}{2}(\varepsilon_k^{(\alpha,\gamma)} + \varepsilon_k^{(\alpha,\beta)} + \varepsilon_k^{(\alpha,\delta)} + h\cos\theta_\alpha), \\ D_{22}{}^{(k)} &\doteq \tfrac{1}{2}(\varepsilon_k^{(\alpha,\beta)} + \varepsilon_k^{(\beta,\delta)} + \varepsilon_k^{(\beta,\gamma)} + h\cos\theta_\beta), \\ D_{33}{}^{(k)} &\doteq \tfrac{1}{2}(\varepsilon_k^{(\alpha,\beta)} + \varepsilon_k^{(\beta,\delta)} + \varepsilon_k^{(\beta,\gamma)} + h\cos\theta_\beta), \\ D_{44}{}^{(k)} &\doteq \tfrac{1}{2}(\varepsilon_k^{(\gamma,\delta)} + \varepsilon_k^{(\beta,\delta)} + \varepsilon_k^{(\alpha,\delta)} + h\cos\theta_\delta). \end{aligned} \tag{B2}$$

$$\begin{aligned} &D_{12}{}^{(k)} \doteq \tfrac{1}{2} v_k^{(\alpha,\beta)}, \quad D_{13}{}^{(k)} \doteq \tfrac{1}{2} v_k^{(\alpha,\gamma)}, \quad D_{14}{}^{(k)} \doteq \tfrac{1}{2} v_k^{(\alpha,\delta)}, \\ &D_{23}{}^{(k)} \doteq \tfrac{1}{2} v_k^{(\beta,\gamma)}, \quad D_{24}{}^{(k)} \doteq \tfrac{1}{2} v_k^{(\beta,\delta)}, \quad D_{34}{}^{(k)} \doteq \tfrac{1}{2} v_k^{(\gamma,\delta)}. \end{aligned} \tag{B3}$$

The matrix $\mathcal{R}$ has the structure

$$\begin{pmatrix} R_{14} & R_{13} & R_{12} & 0 \\ R_{24} & R_{23} & 0 & R_{21} \\ R_{34} & 0 & R_{32} & R_{31} \\ 0 & R_{43} & R_{42} & R_{41} \end{pmatrix}, \tag{B4}$$

and its elements are

$$\begin{aligned} &R_{12}{}^{(k)} \doteq \tfrac{1}{2} q_k^{(\alpha,\beta)}, \quad R_{13}{}^{(k)} \doteq \tfrac{1}{2} q_k^{(\alpha,\gamma)}, \quad R_{14}{}^{(k)} \doteq \tfrac{1}{2} q_k^{(\alpha,\delta)}, \\ &R_{23}{}^{(k)} \doteq \tfrac{1}{2} q_k^{(\beta,\gamma)}, \quad R_{24}{}^{(k)} \doteq \tfrac{1}{2} q_k^{(\beta,\delta)}, \quad R_{34}{}^{(k)} \doteq \tfrac{1}{2} q_k^{(\gamma,\delta)}. \end{aligned} \tag{B5}$$

The diagonalization of H_{SW} is equivalent to an inner automorphism of the algebra on itself. In other words, we can define the unitary operator $\mathbf{U} \doteq \Pi_k U_k$, with

$$U_k \doteq e^{G_k}, \tag{B6}$$

where the anti-Hermitian operator G_k is a linear combination of the non-Cartan generators of the algebra

$$G_k \doteq \sum_{r,s} [\psi_{r,s}(X_{rs} - X^{rs}) + \psi_r{}^s(X_r{}^s - X_s{}^r)]. \tag{B7}$$

The rotation of the Hamiltonian through **U** defines an inner automorphism of the algebra generalizing the Bogoliubov transformation

$$\begin{aligned} &\mathbf{U} H_{SW} \mathbf{U}^{-1} = \sum_k \exp(adG_k) H_k, \\ &\exp(adG_k) H_k \doteq U_k H_k U_k{}^{-1} \\ &\qquad = H_k + \sum_n \frac{1}{n!} [\cdots [G_k, [G_k, H_k]] \cdots]. \end{aligned} \tag{B8}$$

For the closure property of the Lie algebras Eqs. (B8) still produce an element of $\mathcal{A}$; however, we can fix the ψ_{rs}'s and the $\psi_r{}^s$'s in such a way as to put to zero the coefficients of the off-diagonal part of the Hamiltonian. As a final result H_{SW} becomes proportional to the generators of the Cartan subalgebra of $\mathcal{A}$:

$$\mathbf{U} H_{SW} \mathbf{U}^{-1} = H_{\text{diag}} = \sum_{r=1}^{4} \omega_k{}^{(r)} X_r{}^r. \tag{B9}$$

In the present case H_{SW} is diagonal after having solved 16 coupled nonlinear equations. Being interested in the eigenvalues only, we are allowed to use the faithful representation of $\mathcal{A}$ to find the spectrum of the Hamiltonian diagonalizing the matrix $\mathcal{M}(H_{SW})$ instead of H_{SW} as an operator using Eq. (B8). These operations are equivalent because the diagonalization procedure involves commutators between the elements of the algebra only.

[1] Proceedings of the NATO Advanced Research Workshop on Coherence in Superconducting Networks, edited by J.E. Mooij and G. Schön [Physica B **152**, xxx (1988)].

[2] *Proceedings of the Conference on Macroscopic Quantum Phenomena and Coherence in Superconducting Networks*, edited by C. Giovannella and M. Tinkham (World Scientific, Singapore, 1995).

[3] L.J. Geerligs, M. Peters, L.E.M. de Groot, A. Verbruggen, and J.E. Mooij, Phys. Rev. Lett. **63**, 326 (1989); H.S.J. van der Zant, L.J. Geerligs, and J.E. Mooij, Europhys. Lett. **19**, 541 (1992); P. Delsing, C.D. Chen, D.B. Haviland, Y. Harada, and T. Claeson, Phys. Rev. B **50**, 3959 (1995).

[4] K.B. Efetov, Sov. Phys. JETP **51**, 1015 (1980); S. Doniach, Phys. Rev. B **24**, 5063 (1981); R. Fazio and G. Schön, *ibid.* **43**, 5307 (1991).

[5] M.P.A. Fisher, B.P. Weichman, G. Grinstein, and D.S. Fisher, Phys. Rev. B **40**, 546 (1989); G.G. Batrouni, R.T. Scalettar, and G.T. Zimanyi, Phys. Rev. Lett. **65**, 1765 (1990); W. Krauth and N. Trivedi, Europhys. Lett. **14**, 627 (1991).

[6] M.P.A. Fisher, G. Grinstein, and S.M. Girvin, Phys. Rev. Lett. **64**, 587 (1990).

[7] X.G. Wen and A. Zee, Int. J. Mod. Phys. B **4**, 437 (1990).

[8] M.-C. Cha, M.P.A. Fisher, S.M. Girvin, M. Wallin, and A.P. Young, Phys. Rev. B **44**, 6883 (1991); M. Wallin, E.S. Sørensen, S.M. Girvin, and A.P. Young, *ibid.* **45**, 13 136 (1992); G.G. Batrouni, B. Larson, R.T. Scalettar, J. Tobochnik, and J.

Wang, *ibid.* **48**, 9628 (1993); A. van Otterlo, K.-H. Wagenblast, R. Fazio, and G. Schön, *ibid.* **48**, 3316 (1993); R. Fazio and D. Zappalà, *ibid.* **53**, 8883 (1996).

[9] S. Teitel and C. Jayaprakash, Phys. Rev. B **27**, 598 (1983); Phys. Rev. Lett. **51**, 1999 (1983); T.C. Halsey, Phys. Rev. B **31**, 5728 (1985); W.Y. Shih and D. Stroud, *ibid.* **30**, 6774 (1984); W.Y. Shih and D. Stroud, *ibid.* **28**, 6575 (1983); D. Ariosa, A. Vallat, and H. Beck, J. Phys. (Paris) **51**, (1990).

[10] R.S. Fishman and D. Stroud, Phys. Rev. B **37**, 1499 (1987); in this work on-site Coulomb repulsion and no gate voltage were assumed.

[11] A.F. Andreev and I.M. Lifshitz, Sov. Phys. JETP **29**, 1107 (1969)

[12] K.S. Liu and M.E. Fisher, J. Low Temp. Phys. **10**, 655 (1973).

[13] H. Matsuda and T. Tsuneto, Suppl. Prog. Theor. Phys. **46**, 411 (1970).

[14] C. Bruder, R. Fazio, and G. Schön, Phys. Rev. B **47**, 342 (1993).

[15] E. Roddick and D.H. Stroud, Phys. Rev. B **48**, 16 600 (1993); E. Sørensen and E. Roddick, *ibid.* **53**, 8867 (1995).

[16] A. van Otterlo and K-H. Wagenblast, Phys. Rev. Lett. **48**, 1660 (1994).

[17] R.T. Scalettar, G.G. Batrouni, A.P. Kampf, and G.T. Zimanyi, Phys. Rev. B **51**, 8467 (1995).

[18] P. Niyaz, R.T. Scalettar, C.Y. Fong, and G.G. Batrouni, Phys. Rev. B **44**, 7143 (1991).

[19] A. Stern, Phys. Rev. B **50**, 10 092 (1994); A.A. Odintsov and Yu. N. Nazarov, Physica B **203**, 513 (1994); Phys. Rev. B **51**, 1133 (1995); M.Y. Choi, *ibid.* **50**, 10 088 (1994); M. C. Diamantini, P. Sodano, and C. A. Trugenberger Phys. Rev. Lett. **75**, 3517 (1995).

[20] B.G. Wybourne, *Classical Groups for Physicist* (Wiley, New York, 1974).

[21] A. Montorsi, M. Rasetti, and A.I. Solomon, Phys. Rev. Lett. **59**, 2243 (1987).

[22] A.M. Perelomov, *Generalized Coherent States and their Applications* (Springer, Berlin, 1986).

[23] R. Gilmore, *Lie Groups, Lie Algebra, and Some of Their Applications* (Wiley, New York, 1974).

[24] Y.C. Cheng, Phys. Rev. B **23**, 157 (1981).

[25] G. Falci, R. Fazio, A. Tagliacozzo, and G. Giaquinta, Europhys. Lett. **30**, 169 (1995).

[26] W.-M. Zhang, D.H. Feng, and R. Gilmore, Rev. Mod. Phys. **62**, 867 (1990).

[27] G. Chester, Phys. Rev. A **2**, 256 (1970).

[28] A.I. Solomon, J. Phys. A **14**, 2177 (1981).

[29] L. Amico, M. Rasetti, and R. Zecchina, Physica A **230**, 300 (1996).